Journal of Disability Research

2023 | Volume 2 | Issue 3 | Pages: 70–85
DOI: 10.57197/JDR-2023-0041

Multi-targeted Virtual Screening of Phytocompounds of *Rauwolfia serpentina* Against Caspase-8, BACE, and AChE for the Treatment of Neurodegenerative Diseases

Nada H. Aljarba[1], Faizan Abul Qais[2,*], Reem A. Alqahtani[3] and Saad Alkahtani[3]

[1]Department of Biology, College of Science, Princess Nourah bint Abdulrahman University, P. O. Box 84428, Riyadh 11671, Saudi Arabia
[2]Department of Agricultural Microbiology, Faculty of Agricultural Sciences, Aligarh Muslim University, Aligarh 202002, India
[3]Department of Zoology, College of Science, King Saud University, P. O. Box 2455, Riyadh 11451, Saudi Arabia

Correspondence to:
Faizan Abul Qais*, e-mail: faizanabulqais@gmail.com, Tel: +91-9808185856, Fax: +91-571-2703516

Received: July 29 2023; Revised: September 30 2023; Accepted: October 3 2023; Published Online: October 19 2023

ABSTRACT

Brain-related disorders that are associated with neurodegeneration are collectively termed neurodegenerative disorders (NDs). They pose a serious concern for human health, especially among older people. Nearly 47 million individuals are living with dementia; this is expected to increase three times by 2050. The blood–brain barrier is considered a major challenge in the development of drugs against NDs. *Rauwolfia serpentina* is a medicinal plant traditionally used for the treatment of NDs such as schizophrenia, anxiety, insomnia, and mental illness. In this study, the compounds of this plant were examined against caspase-8, β-secretase, and acetylcholinesterase of NDs. The detailed toxicological profile, adsorption, distribution, metabolism, excretion (ADME) properties, and pharmacokinetics were predicted, followed by virtual screening with molecular docking. Based on the toxicity, drug likeliness, pharmacokinetics, anti-neurodegenerative activity, binding site in target proteins, and binding energy, alstonine and rauwolscine were identified as lead compounds. The molecular dynamics simulation of lead compounds was also performed to study their dynamics and stability by mimicking the physiological conditions. Only three compounds showed Ames toxicity, and none of the compounds were predicted to be human Ether-à-go-go-Related Gene (hERG) I inhibitors or cause oral rat acute toxicity. Alstonine was predicted to be active against Alzheimer's disease and neurodegenerative diseases, and rauwolscine was predicted to be active against acute neurologic disorders. The energies for interaction of alstonine and rauwolscine were −10.1 and −8.7 kcal/mol, respectively. Molecular simulation analysis confirmed the stable nature of both the ligands with all three target proteins under physiological conditions. The data of this study highlight the potency of alstonine and rauwolscine for the treatment of NDs, and these compounds could be developed as effective drugs after careful *in vivo* examination.

KEYWORDS

Rauwolfia serpentina, sarpgandha, Alzheimer's disease, virtual screening, molecular dynamics simulation, neurodegenerative disease

INTRODUCTION

The majority of brain-related illnesses are marked by neurodegeneration, recognized as the fundamental pathological alteration (Merelli et al., 2013). Neurodegenerative disorders (NDs), including dementia and Alzheimer's disease, continue to pose substantial clinical challenges, particularly among the elderly population (Choonara et al., 2009; Rapp et al., 2015). A major obstacle in treating NDs is the formidable blood–brain barrier. Surgical and invasive approaches have demonstrated partial success; however, their adoption in clinical practice is constrained due to apprehensions about potential long-term harm to the integrity of the brain barrier (Lamptey et al., 2022). Neurons are crucial for proper functioning of human brain as they play a vital role in the communication system (Jefferys and Cooper, 2007; van den Heuvel and Sporns, 2013). In childhood, the majority of neurons are generated by neural stem cells, but their numbers significantly decrease in adulthood (Ganat et al., 2006). Neurodegeneration, which refers to the gradual loss of neurons, their structure and/or function, stands as a central factor in the pathophysiology of numerous brain disorders (Przedborski et al., 2003). Consequently, it presents a significant health concern. Neurodegeneration manifests through synaptic dysfunction, disruption of neural networks, and the accumulation of chemically modified protein variants in the brain (Hoover et al., 2010; Milnerwood and Raymond, 2010; Scott et al., 2010; Kovacs, 2019). All conditions marked by neurodegeneration fall under the collective term "neurodegenerative disorders (NDs)". Common examples of NDs

encompass Alzheimer's disease (AD), Parkinson's disease, amyotrophic lateral sclerosis, prion disease, Huntington's disease, motor neuron disease, spinocerebellar ataxia, and spinal muscular atrophy (Martin, 1999; Lamptey et al., 2022). Around 47 million individuals are currently living with dementia, and projections suggest that this figure will triple by the year 2050 (Ahmad et al., 2020).

Activation of caspases is a significant event in the apoptotic pathway, triggering the breakdown of proteins in neurons. Previous understanding suggested that AD is characterized by individual occurrences of plaques and tangles without involving activation of caspases. Nonetheless, recent findings suggest that plaques, tangles, and caspase activation all play a combined role in the progression of AD, and Tau proteins cleaved by caspases may potentially initiate or exacerbate the formation of Tau tangles (Cotman et al., 2005). Caspase-8, a large molecule, plays a notable role in AD and is stimulated by amyloid-β 1-40 ($A\beta_{1-40}$) to induce apoptosis. Caspase-8 assumes a pivotal role in AD as it participates in the degradation of amyloid precursor proteins (APPs) during apoptosis, ultimately resulting in elevated amyloid-beta peptide production (Jamal et al., 2019). It is suggested that inhibiting caspase-8 could potentially suppress neuronal apoptosis and alleviate movement impairments associated with AD (Qian et al., 2015).

The cleavage of APP in amyloid cascade is primarily mediated by β-secretase-1 (BACE1) enzyme, resulting in the production of $A\beta_{1-40}$ and $A\beta_{1-42}$ (Goedert and Spillantini, 2006). This process holds a pivotal position in the pathophysiology of AD, as it is accountable for the development of amyloid plaques, which give rise to the disease's symptoms. Elevated levels of monomeric A-β lead to its aggregation to form amyloid fibrils, known to form plaques, cause neurotoxicity, and initiate Tau pathology, ultimately resulting in neurodegeneration and cell death (Kametani and Hasegawa, 2018). Alterations in the expression of BACE1, whether elevated or reduced, is linked with pathological conditions like AD, disruptions in synaptic plasticity, and memory impairment, indicating a tightly regulated mechanism controlling its expression (Faghihi et al., 2008). The altered expression of BACE1 is associated with the pathophysiology of several human diseases, particularly AD and various types of cancer (Sayad et al., 2022). Consequently, β and γ-secretases have emerged as promising molecular targets for newer therapies aimed at addressing NDs (Mouchlis et al., 2020).

NDs are linked with the cholinergic system, which depends on the neurotransmitter acetylcholine (ACh) and its degradation by the enzyme acetylcholinesterase (AChE). AChE inhibitors are frequently utilized in the therapeutic management of these disorders. Notably, AChE plays multiple roles beyond ACh breakdown, encompassing inflammation, morphogenic and adhesion processes, and cellular apoptosis, apart from its involvement in oxidative stress. In the presence of neurodegenerative diseases and depressive disorders, there is an occurrence of inflammation, increased cellular apoptosis, and heightened oxidative stress (Ruz et al., 2020). Hence, inhibition of AChE is also considered as an effective target in the management of NDs (Walczak-Nowicka and Herbet, 2021).

In the present era, there is a global trend toward utilizing herbal medications, which harness the power of bioactive compounds, for disease treatment (Tiwari, 2008). *Rauwolfia serpentina*, a member of the Apocynaceae family, holds significant importance in the field of pharmaceuticals due to its wide range of therapeutic properties (Kumari et al., 2013; Ali et al., 2022). This plant has exhibited efficacy in addressing hypertension and psychiatric conditions like schizophrenia, anxiety, insomnia, and various mental illnesses, among other disorders (Qureshi and Udani, 2009). The roots of this plant have yielded numerous indole alkaloids and related compounds that possess noteworthy biological activities (Itoh et al., 2005). An *in vitro* investigation has documented the antioxidant and antimicrobial properties of the leaf extract obtained from this particular plant (Dey and De, 2011). The primary alkaloid of *R. serpentina* is reserpine, and it can be found in the plant's roots, leaves, and stems.

In this study, we have examined the effect of phytocompounds of *R. serpentina* against the multiple targets of NDs. A total of 29 compounds, especially alkaloids, were used to target caspase-8, β-secretase (BACE), and AChE. The detailed toxicological profile of compounds was predicted along with their ADME properties. Their pharmacokinetics and drug-like properties were also predicted. The virtual screening was done with molecular docking. Based on the toxicity, drug likeliness, pharmacokinetics, anti-neurodegenerative activity, binding site in target proteins, and binding energy, two compounds (alstonine and rauwolscine) were found to be lead compounds. The molecular dynamics (MD) simulation of lead compounds was also performed to study their dynamics and stability by mimicking the physiological conditions.

MATERIALS AND METHODS

Preparation of a library of compounds of *R. serpentina*

A total of 29 compounds of *R. serpentina* were obtained by digging into the literature of this plant (Kumari et al., 2013, 2021; Pathania et al., 2015). The SDF format files of the phytocompounds were obtained from PubChem and their details are enlisted in Supplementary Table S1. The SDF files were converted to PDB using Chimera 1.14. The PDB files were used to prepare the PDBQT files using AutoDockTools-1.5.6 for molecular docking (Morris et al., 2009).

Prediction of ADMET properties using pkCSM

For the prediction of adsorption, distribution, metabolism, excretion, toxicity (ADMET) properties, Canonical simplified molecular-input line-entry system (SMILES) were obtained from the PubChem database. The Canonical SMILES served as input for the prediction of ADMET properties using pkCSM (Pires et al., 2015). A large number of parameters of ADMET were obtained from pkCSM in which few were selected for the analysis. ADMET properties give useful information regarding the efficacy and integrity of compounds which may be important in the early stages of compound selection for drug discovery. The extent of

toxicity of compounds both to human and animal model can be predicted using this server. Before examining the effect of a drug, information regarding their adverse or toxic effect is important in drug designing (Wang et al., 2015).

Prediction of drug likeliness and pharmacokinetics using SwissADME

The Canonical SMILES obtained from the PubChem database also served as the input for the prediction using SwissADME (Daina et al., 2017). Two groups of predictions were taken from SwissADME, which include drug-like properties and pharmacokinetics. There are numerous rules, such as Lipinski, Ghose, Veber etc., that a compound should follow before being developed into successful drugs.

Prediction of activity against AD and neurodegenerative diseases

The compounds were also predicted for their ability in treating AD, NDs, and acute neurologic disorders. The Canonical SMILES were used as the input for these predictions using PASS Online server of Way2Drug (Filimonov et al., 2014). This server predicts a large number of biological activities in which AD, NDs, and acute neurologic disorders were selected for this study. The server predicts the probability of compounds either being active (Pa) or inactive (denoted as Pi). Pa is the estimation of chances of belonging of a compound in a sub-class of active compounds. Likewise, Pi is the estimation of chances of belonging of a compound in the sub-class of inactive compounds.

Preparation of target proteins

Three different target proteins of neurodegenerative diseases, viz. caspase-8 (1QTN), BACE (1W51), and AChE (4EY7), were taken from the Protein Data Bank. Both A and B chains of caspase-8 were used for docking. The structures were cleaned using all other atoms such as ions, water, inhibitors etc. except protein. The missing residues in the crystal structure of BACE and AChE were modeled using Modeller 10.4 (Šali and Blundell, 1993). The X-ray crystal structures contained inhibitors that also served as control.

Virtual screening using molecular docking

The docking procedure was first validated by extracting the inhibitors from their respective crystal structure and then redocking. The preparation of receptors/proteins for molecular docking was done using AutoDockTools-1.5.6 (Morris et al., 2009). First, the polar hydrogen atoms were added to the protein structures followed by adding the Kollman changes. The structure was saved into the PDBQT format prior to docking. The spacing of grid was fixed at Å. The details of grid size and grid center are given in Supplementary Table S2. The molecular docking was done with AutoDock Vina (Trott and Olson, 2009). The PDB files of compounds/inhibitors were opened as ligand and then their roots were detected using AutoDockTools-1.5.6. This makes the ligand flexible and helps in getting better docked conformations. Post molecular docking analysis was done using PyMOL and Discovery Studio 2021.

MD simulation

Based on the toxicity, drug likeliness, pharmacokinetics, anti-neurodegenerative activity, binding site in target proteins, and binding energy, two compounds were selected as lead compounds. The top lead compounds are alstonine and rauwolscine. The complexes of these lead compounds were further studied for stability and dynamics using MD simulation. The MD simulation was carried out with gromacs 2018.1 (Berendsen et al., 1995). The topology of target proteins was produced with pdb2gmx utility of gromacs-2018.1. The topology of ligands/compounds were produced with Antechamber packages of AmberTools21 (Sousa da Silva and Vranken, 2012). Amber99sb-ILDN force field was used to simulate the complexes (Wang et al., 2004). The topology of ligands and proteins was merged manually to make the topology of complex. One inhibitor (tetrapeptide inhibitor Ace-IETD-aldehyde) of caspase-8 is also included that served as control. Triclinic boxes were created around the structures in which the distance between structure and edge of box was 1.0 nm to satisfy periodic boundary conditions (PBCs). The systems were solvated in water using the TIP3P water model and charges on systems were neutralized by equal amount of counter ions (Na or Cl) and then 150 mM NaCl was added to the box to mimic the physiological salt concentration. The systems' energy was minimized through a maximum of 50,000 steps to eliminate the relatively weak van der Waals forces. Two set of equilibrations were done before the simulation. First equilibration was done using NVT ensemble (constant volume, number of particles, and temperature) at 310 K using a thermostat called V-rescale for 1000 ps. Second equilibration was done using NPT ensemble (constant number of pressure, particles, and temperature) at 1.0 bar using Parrinello-Rahman barostat for another 1000 ps (Parrinello and Rahman, 1981). The equilibrated systems were used for the 100 ns simulation of all systems. The PBC corrections were made to all trajectories prior to the analysis. The proteins alone were also simulated that served as control. Most of the analysis was done with the gromacs utilities. The components of binding energy were computed with molecular mechanics poisson-boltzmann surface area (MM-PBSA) calculation with the g_mmpbsa package (Kumari et al., 2014).

RESULTS AND DISCUSSION

ADMET properties of the phytocompounds of *R. serpentina*

First, toxicity of all compounds was predicted using pkCSM. We considered Ames toxicity, hepatotoxicity, hERG I

inhibition, oral rat acute toxicity, *Tetrahymena pyriformis* toxicity, skin sensitization, and minnow toxicity. The data were interpreted as per the manual provided by the server. The predicted toxicological properties are listed in Table 1. Only three compounds were found to show the Ames toxicity. None of the compounds were predicted to be hERG I inhibitors and none showed oral rat acute toxicity. Only one compound (2,6-Dimethoxybenzoquinone) was sensitive to skin and showed *T. pyriformis* toxicity. 11 phytocompounds were predicted to be hepatotoxic. 15 compounds showed minnow toxicity. pkCSM predicted the LC_{50} values for the death of flathead minnows, and the model was built with the LC_{50} measurements of 554 compounds. A study conducted on the anticytotoxic and antigenotoxic effects revealed that the root extract of *R. serpentina* protected chromium (IV)-induced micronuclei induction, biochemical alterations of liver enzymes, and chromosomal aberrations in *Channa punctatus* (Trivedi et al., 2021).

The ADME properties of compounds were also predicted using pkCSM. Two parameters of absorption (intestinal absorption and water solubility), three parameters of distribution (volume of distribution/VDss, central nervous system (CNS) permeability, and fraction unbound), one parameter each for metabolism (CYP3A4 Inhibitor) and excretion (Renal OCT2 substrate) are analyzed here. The predicted ADME properties are listed in Table 2. Only one compound (rutin) exhibited very less intestinal absorption (23.446%). Most of the compounds were either moderately soluble or poorly soluble in water. Only one compound (renoxidine) showed good distribution; the rest of compounds were moderate or poor. Six compounds were CNS permeable, and five compounds exhibited 50% or more fraction unbound value. Six compounds were predicted to be CYP3A4 inhibitors and substrates for renal OCT2.

Drug-like properties and pharmacokinetics

The drug-like properties and pharmacokinetics of compounds were predicted using SwissADME. The drug-like properties of compounds of *R. serpentina* are listed in Supplementary Table S3. Lipinski's rule of five, commonly known as Pfizer's rule of five, is a thumb rule for the evaluation of drug likeness that a certain compound should exhibit for being able to be orally administered in humans. Christopher A. Lipinski formulated this rule in 1997, drawing upon the observation that the majority of

Table 1: Assessment of the toxicity of different bioactive compounds of *Rauwolfia serpentina* using the pkCSM webserver.

Phytocompounds of *R. serpentina*	Ames Tox	hERG I inhibitor	ORAT (LD_{50}) (mg/kg)	Hepatotoxicity	SS	TPT (log μg/L)	MT (log mM)
Raunescine	No	No	15.72	Yes	No	0.285	–1.476
Reserpinine	No	No	19.56	No	No	0.286	–0.015
Alstonine	No	No	12.80	Yes	No	0.887	0.332
Rauwolscine	No	No	10.43	No	No	0.339	–0.165
Rescinnamidine	No	No	19.66	No	No	0.286	–0.065
Yohimbine	No	No	10.43	No	No	0.339	–0.165
Renoxidine	No	No	17.87	No	No	0.286	–1.19
Deserpidine	No	No	17.46	No	No	0.288	–0.094
Ajmalicidine	No	No	10.36	Yes	No	0.67	0.61
Isorauhimbine	No	No	10.43	No	No	0.339	–0.165
Raucaffricine	Yes	No	12.78	Yes	No	0.285	3.741
Reserpine	No	No	18.00	No	No	0.286	0.303
Serpentine	No	No	10.22	Yes	No	0.569	–2.181
Isosandwicine	No	No	9.85	Yes	No	0.289	1.196
Tetraphylline	No	No	11.62	Yes	No	0.602	–0.265
Rutin	No	No	15.21	No	No	0.285	7.677
Isoajmaline	No	No	9.85	Yes	No	0.289	1.196
Rauhimbine	No	No	10.43	No	No	0.339	–0.165
Papaverine	No	No	7.90	Yes	No	0.454	0.16
Raupine	Yes	No	8.29	No	No	0.318	0.786
Kaempherol	No	No	7.01	No	No	0.312	2.885
2,6-Dimethoxybenzoquinone	No	No	3.43	No	Yes	–0.836	2.929
Reserpiline	No	No	12.80	Yes	No	0.504	–0.048
Thebaine	No	No	8.53	No	No	0.937	1.221
Ajmaline	No	No	9.85	Yes	No	0.289	1.196
17-O-Acetylajmaline	No	No	10.63	No	No	0.287	1.739
Diisobutyl phthalate	No	No	4.43	No	No	1.115	–0.24
Ophioxylin	Yes	No	3.08	No	No	0.714	1.751
7-Dehydrositosterol	No	No	10.51	No	No	0.431	–1.759

Abbreviations: Ames Tox, Ames toxicity; MT, minnow toxicity; ORAT, oral rat acute toxicity; SS, skin sensitization; TPT, *Tetrahymena pyriformis* toxicity.

Table 2: Evaluation of the ADME properties of the phytocompounds of *Rauwolfia serpentina* using the pkCSM web server.

Phytocompounds of *R. serpentine*	Absorption		Distribution			Metabolism	Excretion
	Int Abs	WS (log mol/L)	VDss (log L/kg)	CNS per	FUH	CYP3A4 I	Renal OCT2 substrate
Raunescine	94.90	–4.767	0.554	–3.159	0.033	No	No
Reserpinine	96.81	–5.527	0.32	–3.155	0.023	No	No
Alstonine	97.61	–4.538	0.427	–1.883	0.09	No	No
Rauwolscine	94.70	–3.106	1.335	–2.17	0.509	No	No
Rescinnamidine	96.23	–5.521	0.344	–3.212	0.029	No	No
Yohimbine	94.70	–3.106	1.335	–2.17	0.509	No	No
Renoxidine	100	–5.51	–0.341	–3.449	0	No	No
Deserpidine	100	–5.364	0.483	–3.236	0.021	No	No
Ajmalicidine	94.74	–3.972	0.938	–1.994	0.223	No	No
Isorauhimbine	94.70	–3.106	1.335	–2.17	0.509	No	No
Raucaffricine	71.17	–3.262	0.28	–3.813	0.446	No	No
Reserpine	100	–5.345	0.356	–3.364	0.019	No	No
Serpentine	97.73	–3.715	1.442	–2.123	0.235	Yes	Yes
Isosandwicine	98.07	–2.851	0.728	–1.623	0.403	No	No
Tetraphylline	94.06	–3.861	1.049	–2.156	0.21	No	Yes
Rutin	23.44	–2.892	1.663	–5.178	0.187	No	No
Isoajmaline	98.07	–2.851	0.728	–1.623	0.403	No	No
Rauhimbine	94.70	–3.106	1.335	–2.17	0.509	No	No
Papaverine	95.90	–5.118	–0.027	–2.251	0.102	Yes	No
Raupine	95.35	–3.667	1.573	–2.085	0.373	Yes	Yes
Kaempherol	74.29	–3.04	1.274	–2.228	0.178	Yes	No
2,6-Dimethoxybenzoquinone	100	–0.257	–0.177	–2.94	0.735	No	No
Reserpiline	94.18	–4.119	0.931	–2.306	0.224	No	Yes
Thebaine	97.57	–3.208	1.001	–2.326	0.277	No	Yes
Ajmaline	98.07	–2.851	0.728	–1.623	0.403	No	No
17-O-Acetylajmaline	97.09	–2.892	0.733	–2.387	0.254	No	Yes
Diisobutyl phthalate	95.89	–4.407	–0.117	–2.229	0.103	Yes	No
Ophioxylin	96.25	–2.655	0.14	–2.829	0.448	Yes	No
7-Dehydrositosterol	94.61	–6.753	0.192	–1.705	0	No	No

Abbreviations: CNS per, CNS permeability; CYP3A4 I, CYP3A4 inhibitor; FUH, fraction unbound (human); Int Abs, intestinal absorption (human); WS, water solubility. VDss is for human.

orally administered drugs tend to be moderately lipophilic molecules and are relatively small (Lipinski, 2004). Only rutin showed three violations to Lipinski's rule. Four compounds showed two Lipinski's rule violations and one Lipinski's rule violations. The rest of the compounds did not show violation to Lipinski's rule of five. Similarly, the Ghose filter is another knowledge-based filter that is a representation of drug-like properties used in the designing of chemistry libraries for drug discovery (Ghose et al., 1999). The rules are molecular weight should be between 160 and 480 Daltons; logP should be –0.4 to 5.6, the number of atoms should be 20 to 70, and molar refractivity should lie between 40 and 130. The Ghose filter is more stringent than Lipinski's rule of five and a compound is expected to show more Ghose filter violations than Lipinski's rule of five. Rutin showed four violations to Ghose filter. Out of 29 compounds, 9 compounds showed 3 Ghose filter violations. The rest of compounds were within the range of the Ghose filter.

The pharmacokinetics of compounds were also examined using SwissADME. Three important parameters (blood–brain barrier permeability, gastrointestinal absorption, and P-glycoprotein substrate) are analyzed here. The pharmacokinetic properties of the phytocompounds of *R. serpentina* are listed in Supplementary Table S3. Renoxidine, raucaffricine, rutin, and 7-dehydrositosterol showed gastrointestinal absorption; rest of the compounds were predicted to be of high gastrointestinal absorption. 11 compounds were impermeable to blood–brain barrier. 19 out of 29 were predicted to be substrates for P-glycoprotein. Overall, two lead compounds identified in this study exhibited good drug-like properties and pharmacokinetics, which are important for their ability to be developed as successful drugs.

Prediction of activity against AD and neurodegenerative diseases

The prediction of ability of compounds of *R. serpentina* in the treatment of AD, neurodegenerative diseases, and acute neurologic disorders was also performed and the data are presented in Supplementary Table S4. Four compounds including alstonine were predicted to be active against the neurodegenerative diseases and AD. A total of 10 compounds including rauwolscine were predicted to be active against acute neurologic disorders. The data clearly depict the ability of several phytocompounds of *R. serpentina* to be active against neurological disorders. Alstonine has been found to

be a potent antipsychotic in mice models (Costa-Campos et al., 1998). Moreover, there is also report on the anxiolytic properties of alstonine (Costa-Campos et al., 2004).

Molecular docking

First, the molecular docking procedure was validated by extracting the inhibitor/ligand attached to the crystal structure of target proteins. The ligands were docked at the same position where they were present in the crystal structure. The molecular docking of the phytocompounds of *R. serpentina* was performed against three different targets of neurodegenerative diseases. The values of binding energies, binding constants, inhibition constants, and binding sites are listed in Table 3. Out of all compounds, alstonine exhibited the highest affinity to AChE with a binding constant of −10.1 kcal/mol. Similarly, yohimbine showed highest affinity toward BACE, and raunescine showed highest affinity toward caspase-8. Based on the toxicity, drug likeliness, pharmacokinetics, anti-neurodegenerative activity, binding site in target proteins, and binding energy, two compounds were selected as lead compounds. The top lead compounds are alstonine and rauwolscine. Hence, the interaction of only these two compounds with target proteins is discussed in this section. Alstonine formed two hydrogen bonds with Try72, Gly121, and Tyr124 of AChE with bond lengths of 3.28 Å, 3.26 Å and 2.44 Å, respectively (Fig. 1a). The complex was also found to be stabilized by hydrophobic bonds that involved Trp86, His447, Tyr337, Tyr341, Tyr72, and Try124. Moreover, there was also involvement of van der Waals forces. In the AChE–rauwolscine complex, two hydrogen bonds were established that included Ser293 and Tyr341. The complex was further stabilized by van der Waals interaction (Gln291, Leu289, Val294, Arg296, Phe295, and Phe338) and hydrophobic interactions (Trp286) as presented in Figure 1b. It is interesting to note that both the ligands interacted at the site where its inhibitor (donepezil) binds. The active site of AChE is comprised of certain residues including Tyr72, Tyr124, Leu289, Trp286, Ser293, Phe295, Val294, Arg296, Tyr337, Phe297, Phe338, Gly342, Tyr341 etc. (Arulraj et al., 2020). The interaction of alstonine and rauwolscine at the active site might lead to the inhibition of this enzyme and may protect against NDs.

Alstonine was found to be docked at the active site of caspase-8 with a binding energy of −7.7 kcal/mol (Fig. 2a). Alstonine formed two hydrogen bonds with Ser411 and Cys360 of caspase-8 at distance of 3.25 Å and 3.47 Å, respectively. Tyr412, Arg413, Arg260, Tyr324 and Leu254 were strengthened by van der Waals interactions. Likewise, Tyr365, Val410, Cys360, His317, and Ile 257 were complexed by hydrophobic forces. The binding energy for the complexation of rauwolscine to caspase-8 was −7.6 kcal/mol (Fig. 2b). The binding constant and inhibition constant for caspase-8–rauwolscine were 37.516×10^4 M^{-1} and 2.666 µM, respectively. Rauwolscine formed three hydrogen bonds, one with Tyr412 and two with Arg413. The complex was further stabilized by van der Waals interactions (Tyr324, Leu254, His317, Arg258, and Ser411) and hydrophobic interactions (Ile257, Val410, Tyr412, and Tyr365).

The binding energy for the docking of alstonine with BACE was obtained as −7.6 kcal/mol. The complex was stabilized by one hydrogen bond (Gly11) with a bond length of 3.71 Å (Fig. 3a). Moreover, there is also involvement of hydroponic bonds (Lys107, Ile110, and Leo30) and van der Waals forces (Ile118, Trp115, Phe108, and Phe47) in the complexation. The interaction diagram of the BACE–rauwolscine complex is presented in Figure 3b. The binding energy was found to be −8.9 kcal/mol. This energy value corresponds to the binding constant and inhibition constant of 337.054×10^4 M^{-1} and 0.297 µM. Rauwolscine formed three hydrogen bonds with Asp32, Asp228, and Thr231 of BACE. There was also involvement of van der forces and a small contribution of hydrophobic interactions. Both the ligands interacted at the active site of BACE which may lead to the inhibition of this enzyme. It is interesting to note that both lead compounds (alstonine and rauwolscine) were docked at the active/catalytic site of target proteins.

MD simulation

Analysis of root-mean square deviation and RMSF

To further investigate the dynamics and stability of hit compounds with the target proteins, MD simulation was performed. The primary investigation was done by calculating the root-mean square deviation (RMSD) of each trajectory with respect to the initial structure and the data are shown in Figure 4a. The RMSD of caspase-8 showed some deviations till 60 ns and it became stable. Likewise, the RMSD of the caspase-8–alstonine complex and the caspase-8–rauwolscine complex also became stable past 60 ns. The average RMSD values of uncomplexed caspase-8, caspase-8–alstonine complex, and caspase-8–rauwolscine complex were found to be 0.388, 0.387, and 0.418 nm, respectively. The average RMSD of caspase-8–inhibitor complex was 0.252 nm. On the contrary, RMSD of BACE and AChE and their complexes became stable during the initial stages of simulation (within 20 ns). The average RMSD of BACE and AChE, and their complexes was less than 0.25 nm. The data give the preliminary idea regarding the stable nature of complexes in a physiological environment. The finding is consistent with an earlier report where the RMSD of caspase-8-rutaecarpine got equilibrated roughly at 0.6 nm (Ahmad et al., 2020).

The fluctuation in residue of all test proteins in the uncomplexed and complexed states was also computed (Fig. 4b). The root mean square fluctuation (RMSF) of nearly all residues of proteins and their complexes with alstonine and rauwolscine was below 0.25 nm. For instance, the average RMSF values of BACE alone, BACE–alstonine complex, and BACE–rauwolscine complex were 0.094, 0.113, and 0.093 nm, respectively. However, the average RMSF of the caspase-8–rauwolscine complex (0.230) was higher than those of caspase-8 alone (0.139) and caspase-8–alstonine complex (0.142). The terminal segments of all proteins exhibited comparatively greater fluctuations, a consequence of their location at the ends, where they tend to experience

Table 3: Binding energy, binding constant, and inhibition constant of compounds of *Rauwolfia serpentina* obtained through molecular docking using AutoDock Vina.

Phytocompounds of *R. serpentina*	AChE				BACE				Caspase-8				Av BE
	BE	K_b ($\times 10^4$ M^{-1})	K_i μM)	BS	BE	K_b ($\times 10^4$ M^{-1})	K_i (μM)	BS	BE	K_b ($\times 10^4$ M^{-1})	K_i (μM)	BS	
Raunescine	–8.1	87.285	1.146	AS	–9	399.066	0.251	AS	–9.4	784.196	0.128	AS	–8.83
Reserpinine	–8.7	240.442	0.416	AS	–8.8	284.679	0.351	AS	–8.6	203.079	0.492	AS	–8.70
Alstonine	–10.1	2557.639	0.039	AS	–7.6	37.516	2.666	AS	–7.7	44.418	2.251	AS	–8.47
Rauwolscine	–8.7	240.442	0.416	AS	–8.9	337.054	0.297	AS	–7.6	37.516	2.666	AS	–8.40
Rescinnamidine	–8.3	122.357	0.817	AS	–8.4	144.869	0.690	AS	–8.4	144.869	0.690	AS	–8.37
Yohimbine	–8.5	171.522	0.583	AS	–9.2	559.416	0.179	AS	–7.2	19.091	5.238	AS	–8.30
Renoxidine	–7	13.619	7.343	AS	–9	399.066	0.251	AS	–8.5	171.522	0.583	AS	–8.17
Deserpidine	–7.2	19.091	5.238	AS	–8.7	240.442	0.416	AS	–8.4	144.869	0.690	AS	–8.10
Ajmalicidine	–7.9	62.266	1.606	AS	–8.2	103.344	0.968	AS	–8.1	87.285	1.146	AS	–8.07
Isorauhimbine	–7	13.619	7.343	AS-N	–8.6	203.079	0.492	AS	–8.6	203.079	0.492	AS	–8.07
Raucaffricine	–7.4	26.762	3.737	AS-N	–8	73.722	1.356	AS	–8.7	240.442	0.416	AS	–8.03
Reserpine	–7	13.619	7.343	AS-N	–8.7	240.442	0.416	AS	–8.4	144.869	0.690	AS	–8.03
Serpentine	–7.9	62.266	1.606	AS	–8.7	240.442	0.416	AS	–7.5	31.686	3.156	AS	–8.03
Isosandwicine	–8.1	87.285	1.146	AS	–8.1	87.285	1.146	AS	–7.6	37.516	2.666	AS	–7.93
Tetraphylline	–8.1	87.285	1.146	AS	–7.5	31.686	3.156	OS	–8.2	103.344	0.968	AS	–7.93
Rutin	–7.3	22.604	4.424	AS-N	–8.8	284.679	0.351	AS	–7.6	37.516	2.666	AS	–7.90
Isoajmaline	–8.1	87.285	1.146	AS	–8.2	103.344	0.968	AS	–7.4	26.762	3.737	AS	–7.90
Rauhimbine	–8.1	87.285	1.146	AS	–8	73.722	1.356	AS	–7.5	31.686	3.156	AS	–7.87
Papaverine	–9.1	472.487	0.212	AS	–7.9	62.266	1.606	AS	–6.4	4.944	20.227	AS	–7.80
Raupine	–8.1	87.285	1.146	AS	–7.5	31.686	3.156	AS	–7.7	44.418	2.251	AS	–7.77
Kaempherol	–8.8	284.679	0.351	AS	–8.1	87.285	1.146	AS	–6.4	4.944	20.227	AS	–7.77
2,6-Dimethoxybenzoquinone	–7.5	31.686	3.156	AS	–8.4	144.869	0.690	AS	–7.2	19.091	5.238	AS	–7.70
Reserpiline	–7.8	52.590	1.901	AS	–7.5	31.686	3.156	OS	–7.7	44.418	2.251	AS	–7.67
Thebaine	–8.5	171.522	0.583	AS	–7.5	31.686	3.156	AS	–6.8	9.715	10.293	AS	–7.60
Ajmaline	–7.6	37.516	2.666	AS	–7.8	52.590	1.901	AS	–7.4	26.762	3.737	AS	–7.60
17-O-Acetylajmaline	–7	13.619	7.343	AS-N	–8	73.722	1.356	AS	–7.4	26.762	3.737	AS	–7.47
Diisobutyl phthalate	–8.5	171.522	0.583	AS	–6.7	8.206	12.187	AS	–5.4	0.913	109.490	AS	–6.87
Ophioxylin	–8.3	122.357	0.817	AS	–6.6	6.931	14.429	AS	–5.6	1.280	78.106	AS	–6.83
7-Dehydrositosterol	–6.1	2.979	33.571	AS	–4.9	0.393	254.740	OS	–4.5	0.200	500.585	OS	–5.17

Abbreviations: AChE, acetylcholinesterase; AS, active site; AS-N, near to active site; Av BE, average binding energy; BACE, β-secretase; BE, binding energy; BS, binding site; K_b, binding constant; K_i, inhibition constant; OS, sites other than the active site.

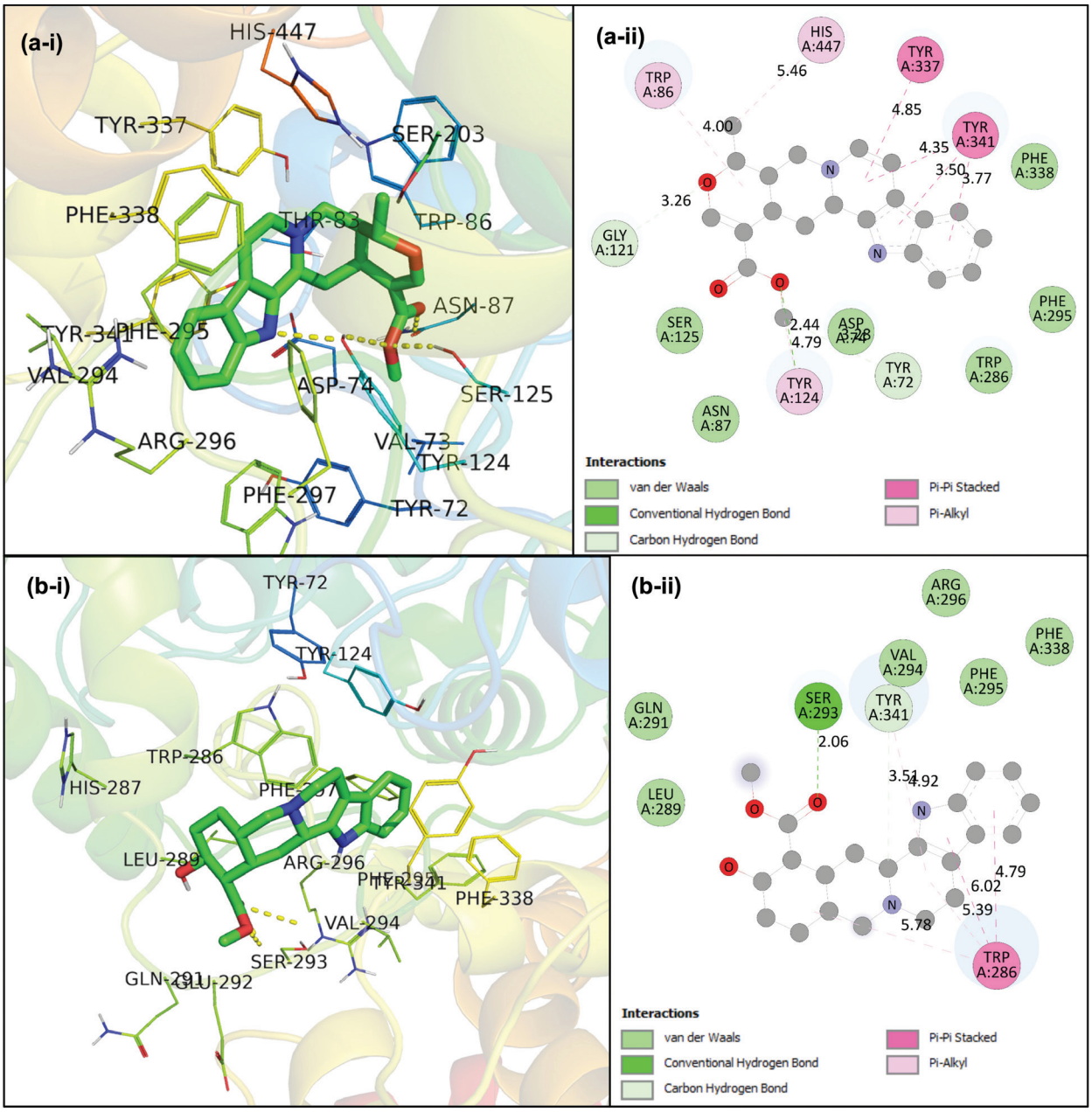

Figure 1: (a) Docked pose of the AChE–alstonine complex. (a-i) Three-dimensional representation of the AChE–alstonine complex; alstonine is shown as blue sticks. AChE is shown as a colored ribbon in which interacting residues are heighted. (a-ii) Two-dimensional representation of the AChE–alstonine complex prepared using Discovery Studio 2021. (b) Docked pose of the AChE–rauwolscine complex. (b-i) Three-dimensional representation of the AChE–rauwolscine complex; rauwolscine is shown as blue sticks. AChE is shown as a colored ribbon in which interacting residues are heighted. (b-ii) Two-dimensional representation of the AChE–rauwolscine complex prepared using Discovery Studio 2021. Abbreviation: AChE, acetylcholinesterase.

more movement in an aqueous environment. In summary, the data indicate that the majority of residues remained stable even when subjected to simulations under physiological conditions, even in the presence of complexes. The RMSF of individual atom of both ligands was also computed to examine their dynamics. The RMSF of ligands is shown in Supplementary Figure S1. Both the ligands showed some fluctuations when complexed with the target proteins. This fluctuation is attributed to the movement of ligands at the binding or active site of proteins (Qais et al., 2023). It is interesting to note that the interaction of rauwolscine with AChE decreased the RMSF of active site residues, which further explains the stability of the complex.

Analysis of protein's compactness and energies

Further examination of the stability of all proteins and their complexes was done by calculating the radius of gyration (R_g), solvent-accessible surface area (SASA), and energies (potential and total). R_g is defined as the root-mean-square

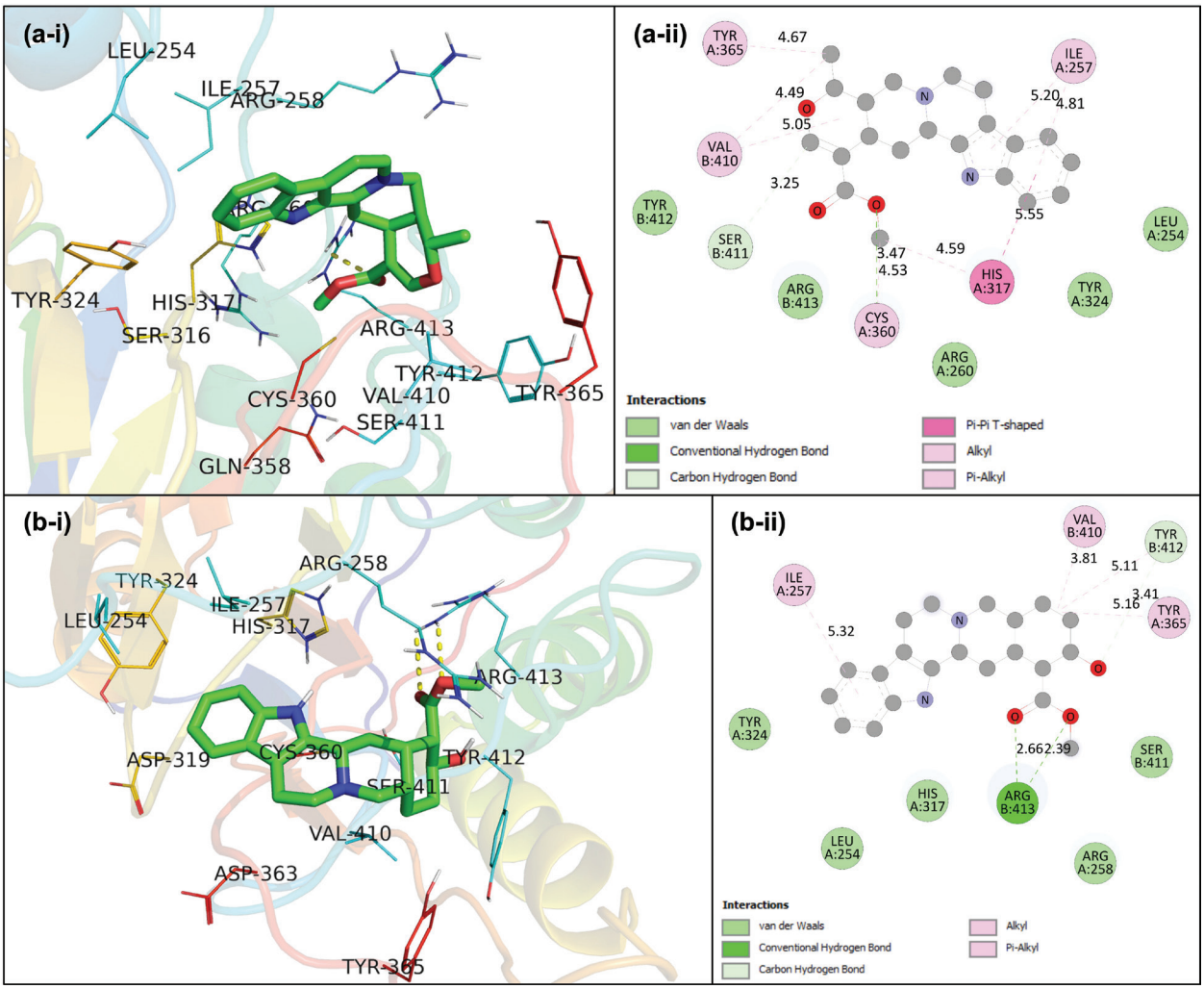

Figure 2: (a) Docked pose of the caspase-8–alstonine complex. (a-i) Three-dimensional representation of the caspase-8–alstonine complex; alstonine is shown as blue sticks. Caspase-8 is shown as a colored ribbon in which interacting residues are heighted. (a-ii) Two-dimensional representation of the caspase-8–alstonine complex prepared using Discovery Studio 2021. (b) Docked pose of the caspase-8–rauwolscine complex. (b-i) Three-dimensional representation of the caspase-8–rauwolscine complex; rauwolscine is shown as blue sticks. Caspase-8 is shown as a colored ribbon in which interacting residues are heighted. (b-ii) Two-dimensional representation of the caspase-8–rauwolscine complex prepared using Discovery Studio 2021.

distance, weighted by mass, between a group of atoms and their shared center of mass. Usually, compact proteins, exhibit lower fluctuations in R_g during simulation while open or expanded proteins show higher alteration in the R_g value over the course of simulation (Qais et al., 2021). This property makes R_g as an important parameter for the examination of stability and structural compactness of proteins during molecular simulations (Fouedjou et al., 2021). The R_g of proteins and complexes with respect to time is shown in Figure 5a. The R_g of BACE and AChE both when uncomplexed and complexed remained almost constant during the entire simulation period. For example, the average R_g values of BACE alone, BACE–alstonine complex, and BACE–rauwolscine complex were found to be 2.078, 2.093, and 2.080 nm, respectively. Similarly, average R_g values of AChE alone, AChE–alstonine complex, and AChE–rauwolscine complex were 2.313, 2.315, and 2.313 nm, respectively. The R_g of caspase and its complexes showed some variations with time but within the acceptable range. In short, calculation of R_g also validates the stability of the complexes.

SASA was also calculated as shown in Figure 5b. The SASA of all systems was quite stable when simulated by mimicking the physiological conditions. The trajectory for SASA of all proteins and complexes was smooth over the course of simulation. The average SASA values of caspase-8 alone, caspase-8–alstonine complex, and caspase-8–rauwolscine complex were 125.774, 127.204, and 125.196 nm^2, respectively. Likewise, average SASA of the caspase-8–inhibitor complex was 127.181 nm^2. Similarly, a negligible difference in the SASA of other two proteins (BACE and AChE) was observed compared to their respective complexes. The examination of SASA further verifies the stability of the hit compounds (alstonine and rauwolscine) in complex with target proteins (caspase-8, BACE, and AChE). The total and potential energies of systems were also computed (Supplementary Fig. S2). Both these energies were constant over the simulation trajectory.

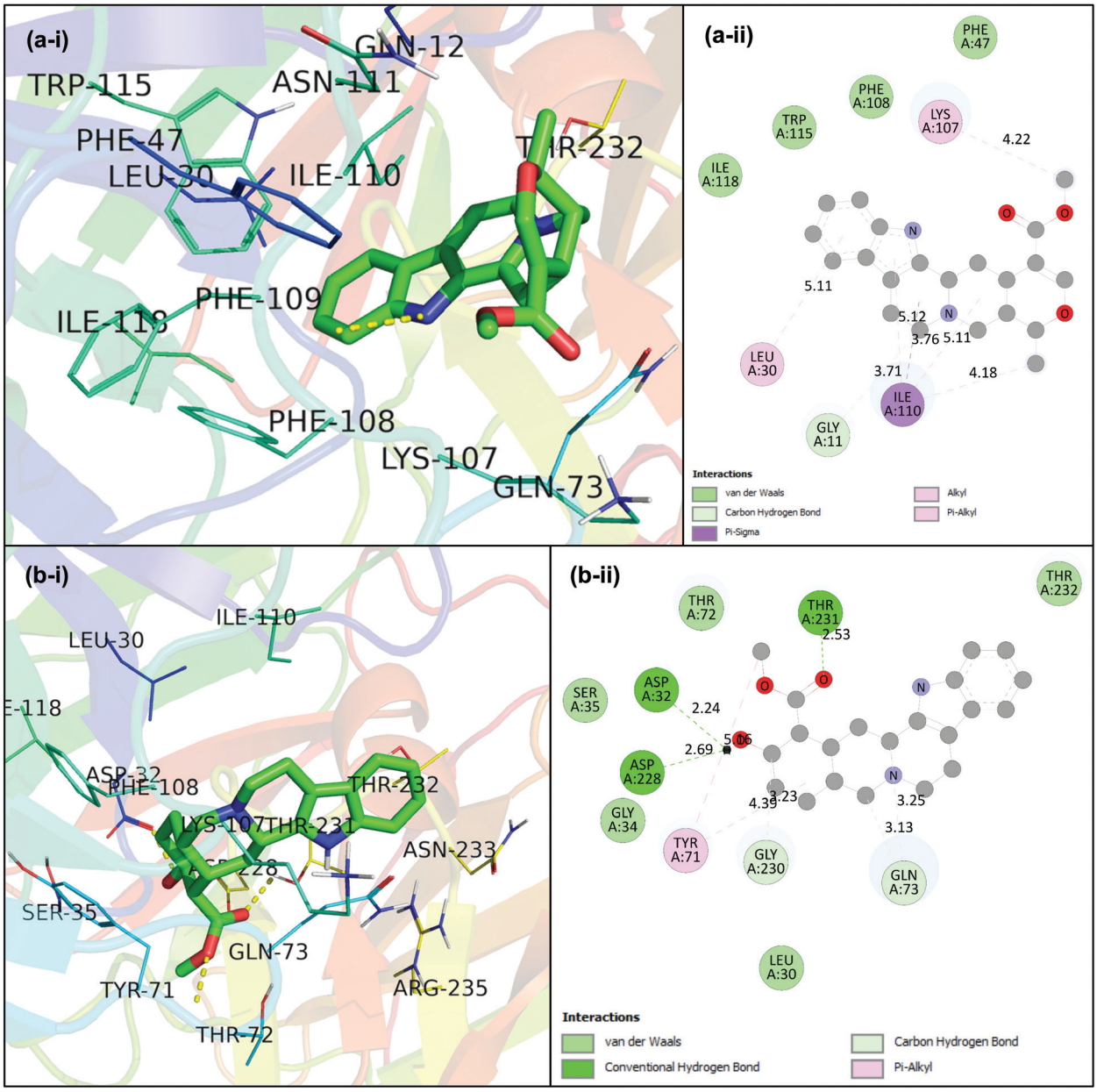

Figure 3: (a) Docked pose of the BACE–alstonine complex. (a-i) Three-dimensional representation of the BACE–alstonine complex; alstonine is shown as blue sticks. BACE is shown as a colored ribbon in which interacting residues are heighted. (a-ii) Two-dimensional representation of the BACE–alstonine complex prepared using Discovery Studio 2021. (b) Docked pose of the BACE–rauwolscine complex. (b-i) Three-dimensional representation of the BACE–rauwolscine complex; rauwolscine is shown as blue sticks. BACE is shown as a colored ribbon in which interacting residues are heighted. (b-ii) Two-dimensional representation of the BACE–rauwolscine complex prepared using Discovery Studio 2021. Abbreviation: BACE, β-secretase.

The analysis of R_g, SASA, and energies confirms that both the ligands formed stable complexes with test proteins under physiological conditions.

Effect of lead compounds on the structure of target proteins

The effect of binding of alstonine and rauwolscine on the structural stability of target proteins was studied by calculating the secondary structures. The average percentage of coils, β-sheets, β-bridges, bends, turns, α-helices, and 3′-helices in caspase-8 alone were found to be 29.78, 18.93, 1.32, 7.51, 15.30, 24.16, and 2.96, respectively (Fig. 6a). All these secondary structural components of caspase-8 remained roughly unchanged when the protein was simulated with alstonine and rauwolscine. The secondary structures of uncomplexed and complexed BACE is shown in Figure 6b. The coils, β-sheets, β-bridges, turns, bends, α-helices, and 3′-helices in BACE were 22.66, 38.65, 0.99, 12.01, 13.98, 7.13, and 4.55, respectively. A negligible effect on the structure of BACE was observed after the complexation of ligands. The amount of secondary structures in AChE alone and in complexes is presented in Figure 6c. A negligible change in the secondary structure of AChE was recorded following the complexation of alstonine and

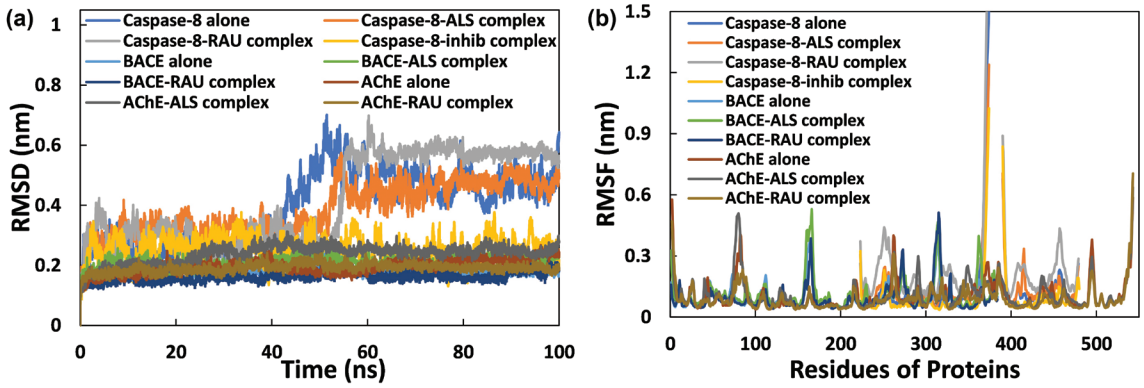

Figure 4: (a) RMSD of caspase-8 alone, caspase-8–alstonine complex, caspase-8–rauwolscine complex, caspase-8–inhib complex, BACE alone, BACE–alstonine complex, BACE–rauwolscine complex, AChE alone, AChE–alstonine complex, and AChE–rauwolscine complex as a function of time. (b) Root-mean square fluctuation of Cα atoms of caspase-8, BACE, and AChE in the absence and presence of alstonine and rauwolscine. Inhib is an inhibitor of caspase-8, i.e. tetrapeptide inhibitor Ace-IETD-aldehyde. Abbreviations: AChE, acetylcholinesterase; BACE, β-secretase; RMSD, root-mean square deviation.

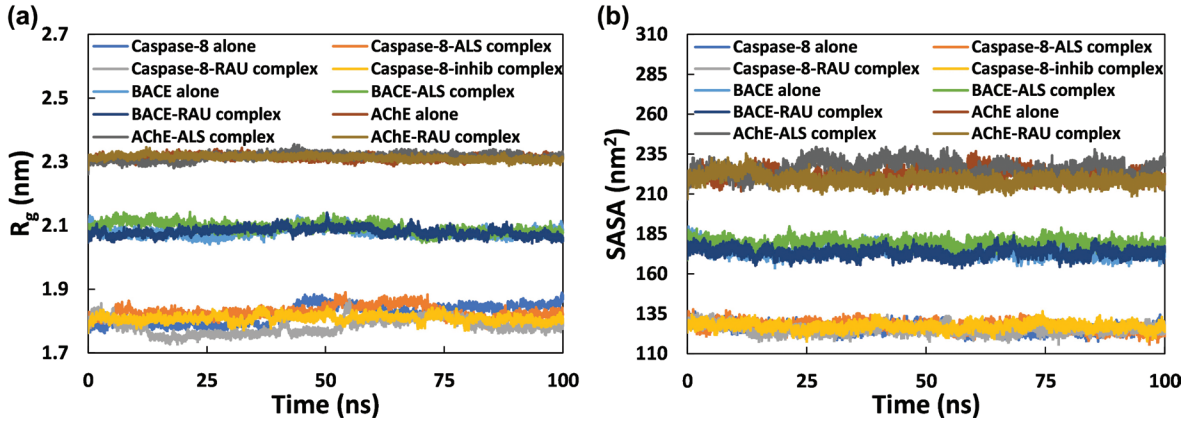

Figure 5: (a) Radius of gyration (R_g) of caspase-8 alone, caspase-8–alstonine complex, caspase-8–rauwolscine complex, caspase-8–inhib complex, BACE alone, BACE–alstonine complex, BACE–rauwolscine complex, AChE alone, AChE–alstonine complex, and AChE–rauwolscine complex as a function of time. (b) SASA of caspase-8 alone, caspase-8–alstonine complex, caspase-8–rauwolscine complex, caspase-8–inhib complex, BACE alone, BACE–alstonine complex, BACE–rauwolscine complex, AChE alone, AChE–alstonine complex, and AChE–rauwolscine complex as a function of time. Inhib is an inhibitor of caspase-8, i.e. tetrapeptide inhibitor Ace-IETD-aldehyde. Abbreviations: AChE, acetylcholinesterase; BACE, β-secretase; SASA, solvent-accessible surface area.

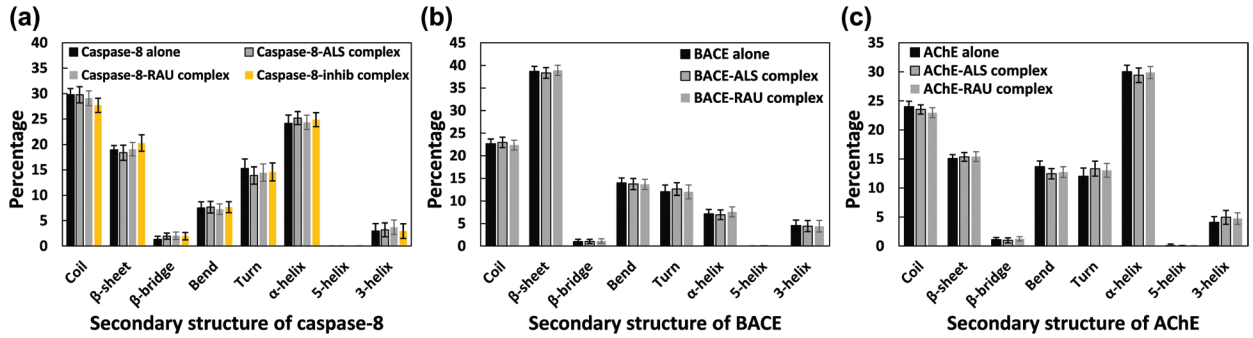

Figure 6: (a) Average secondary structural components of caspase-8 in the absence and presence of alstonine, rauwolscine, and inhibitor of caspase-8 (tetrapeptide inhibitor Ace-IETD-aldehyde). (b) Average secondary structural components of BACE in the absence and presence of alstonine and rauwolscine. (c) Average secondary structural components of AChE in the absence and presence of alstonine and rauwolscine. Abbreviations: AChE, acetylcholinesterase; BACE, β-secretase.

rauwolscine. This discovery aligns with a previous report in which the interaction of F1094-0201 with BACE did not cause any changes in the secondary structural elements (Iqbal et al., 2023). The analysis of the secondary structure confirms that binding of ligands to the target proteins does not alter the stability of target proteins.

Hydrogen bond analysis

The interaction of lead compounds with all three proteins was investigated by computing the hydrogen bonds' number and analyzing the hydrogen bond profile. The number of hydrogen bonds shared between ligands and proteins with respect to time is shown in Supplementary Figure S3. Rauwolscine made a higher number of hydrogen bonds with caspase-8 compared to alstonine. The average number of hydrogen bonds formed by alstonine and rauwolscine with caspase-8 was found to be 0.553 and 1.136, respectively. It is worth noting that the inhibitor (tetrapeptide inhibitor Ace-IETD-aldehyde) of caspase-8 formed an average of 8.88 hydrogen bonds with caspase-8. Similarly, rauwolscine also made more hydrogen bonds with BACE and AChE. The average number of hydrogen bonds formed by alstonine and rauwolscine with BACE was 0.746 and 1.670, respectively. The existence of hydrogen bonds was also calculated over the course of trajectory (Supplementary Fig. S4). Hydrogen bonds between ligands and BACE were consistently observed. A similar result was obtained for caspase. Nonetheless, in the AChE–alstonine complex, hydrogen bonds were present during the initial 30 ns, but they subsequently disappeared. The hydrogen bond occupancy was also calculated for the complexes. Arg413 exhibited hydrogen bond occupancy among all residues of caspase-8 with alstonine. Asn458 exhibited hydrogen bond occupancy in the caspase-8–rauwolscine complex. The residues of BACE that showed highest hydrogen bond occupancy with alstonine and rauwolscine were Lys107 and Gln73, respectively. The data confirm the involvement of hydrogen bonds in the complexation of lead compounds to target proteins.

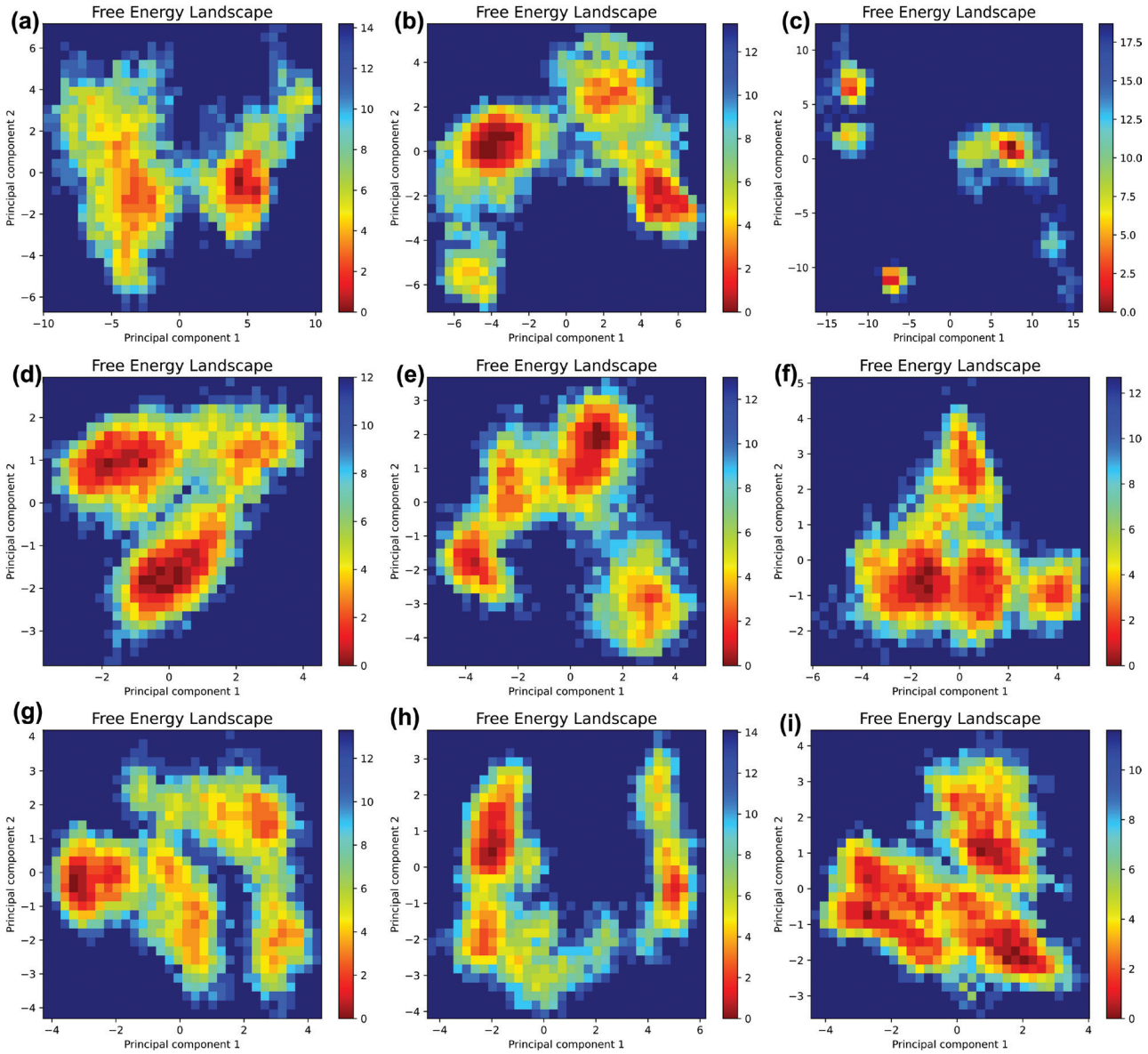

Figure 7: (a) FEL of caspase-8 alone. (b) FEL of the caspase-8–alstonine complex. (c) FEL of the caspase-8–rauwolscine complex. (d) FEL of BACE alone. (e) FEL of the BACE–alstonine complex. (f) FEL of the BACE–rauwolscine complex. (g) FEL of AChE alone. (h) FEL of the AChE–alstonine complex. (i) FEL of the AChE–rauwolscine complex. Abbreviations: AChE, acetylcholinesterase; BACE, β-secretase; FEL, free energy landscape.

Principal component analysis

Principal component analysis (PCA) is a conventional statistical technique used to investigate the extensive movements of proteins. PCA accomplishes this by reducing the dimensionality of data sets while retaining critical information, which is represented as eigenvectors (Siddiqui et al., 2021). PCA was performed to examine the flexibility of proteins in the absence and presence of ligands. The projection of eigenvectors of uncomplexed and complexed proteins in a two-dimensional space is presented in Supplementary Figure S5. The AChE–alstonine complex and the AChE–rauwolscine complex appeared to occupy a similar conformational space in the 2D projection of eigenvectors when compared to AChE alone. This suggests that the flexibility of AChE remained relatively consistent after binding with these ligands. Similar results were observed for BACE. The conformational space occupied by caspase-8–rauwolscine complex was relatively higher compared to caspase-8 alone and the caspase-8–alstonine complex. This shows that binding of rauwolscine to caspase-8 increased the flexibility of this protein.

The eigenvectors were further used to make the free energy landscape (FEL). The FEL of all proteins and their complexes with alstonine and rauwolscine is shown in Figure 7. It is interesting to note that all trajectories reached the energy minimum. However, the position of energy minima differed in the landscapes for the complexes. The coordinates of structures corresponding to free energy minima were extracted and further examined using Ramachandran plots. Ramachandran plots of the lowest energy structures are presented in Supplementary Figure S6. In both caspase-8 alone and the caspase-8–alstonine complex, no residues were located within either the generously allowed or disallowed regions. However, in the caspase-8–rauwolscine complex. Only one residue was situated in the generously allowed region, and none were found in the disallowed region in the caspase-8–rauwolscine complex. This observation indicates the stability of caspase-8 when interacting with these ligands. Three residues were found to lie in the generously allowed region of BACE in uncomplexed and complexed forms. Two amino acids were found in the disallowed regions of AChE alone while the complexation reduced the disallowed residues to one. Overall, these structural analyses further validate the stable nature of complexes.

Analysis of binding energetics

The interaction of ligands with target proteins was further investigated by calculating the involvement of different energies in complexation. In typical ligand–protein complexes, noncovalent interactions like hydrophobic forces, electrostatic interactions, van der Waals interactions, hydrogen bonds, etc. are prevalent. All of these forces impact the overall interaction (Rath et al., 2021). The MM-PBSA binding energies are listed in Figure 8a. Van der Walls forces were prevalent in the complexation of alstonine with caspase-8. Electrostatic forces played a major role in the interaction of rauwolscine with caspase-8 followed by van der Walls forces. For the binding of both ligands with BACE and AChE, electrostatic forces were predominant, followed by the van der Walls forces. Additionally, there was a minor contribution from SASA energy. The polar solvation energy had a detrimental effect on the overall interaction. The binding energies for the interaction of alstonine and rauwolscine with caspase-8 were found to be −29.807 and −41.101 kcal/mol. Similarly, binding energies for the complexation of alstonine and rauwolscine with BACE were −87.059 and −80.340 kcal/mol. The data align with a previous report in which the molecular mechanics generalized born surface area (MM-GBSA) free energy for the binding of F1094-0201 with BACE was determined to be −73.78 kcal/mol (Iqbal et al., 2023).

The MM-PBSA analysis was further employed to pinpoint the primary energy-contributing residues for each of these interactions (Supplementary Fig. S7). Glu249,

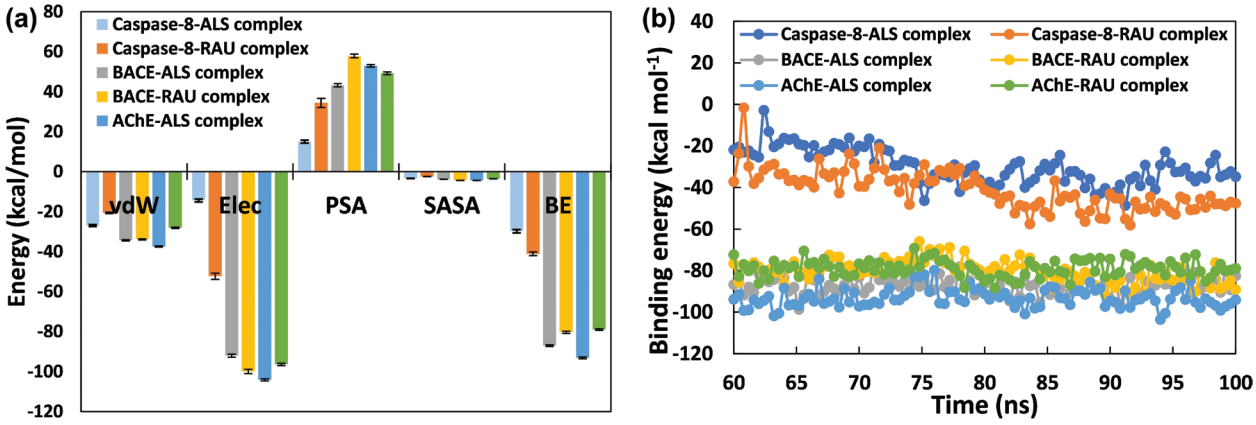

Figure 8: (a) MM-PBSA analysis for different energies of the caspase-8–alstonine complex, caspase-8–rauwolscine complex, BACE–alstonine complex, BACE–rauwolscine complex, AChE–alstonine complex, and AChE–rauwolscine complex. BE, overall binding energy; Elec, electrostatic energy; PSA, polar solvation energy; SASA, SASA energy; vdW, van der Waals energy. (b) Energy per frame of the caspase-8–alstonine complex, caspase-8–rauwolscine complex, BACE–alstonine complex, BACE–rauwolscine complex, AChE–alstonine complex, and AChE–rauwolscine complex of 100 frames from 60 ns to 100 ns of each trajectory. Abbreviations: AChE, acetylcholinesterase; BACE, β-secretase; SASA, solvent-accessible surface area.

Asp259, Asp266, Asp319, Glu330, Asp363, Glu372, Asp374, Glu417, Asp454, Asp455, and Asp479 were major energy contributors for the interaction of alstonine with caspase-8. In the caspase-8–rauwolscine complex, Asp259, Asp266, Glu275, Glu276, Asp285, Asp286, Asp374, Glu417, Glu431, Glu445, Asp454, and Asp479 were the key energy contributors. Asp106 and Asp311 showed highest energy contribution in complexation of alstonine and rauwolscine with BACE, respectively. Similarly, Asp74, Glu81, Glu84, Asp131, Asp134, Glu202, Glu334, Asp349, Glu450, Glu452, Asp460, and Glu469 were key energy-contributing residues for the binding of alstonine with AChE. The energy per frame of 100 snapshots of trajectory from 60 ns to 100 ns was also calculated (Fig. 8b). The energy per frame data also appeared to the stable during the tested period of trajectory and did not show much fluctuations. For example, the minimum and maximum energies of one frame for the BACE–alstonine complex were −98.673 and −76.562 kcal/mol, respectively. Similarly, the minimum and maximum energies of one frame for the AChE–rauwolscine complex were −88.468 and −69.172 kcal/mol. Such small differences in energies are due to the movement of ligand at the binding site.

CONCLUSION

Brain-related disorders, collectively termed as NDs, are becoming a major health concern for older individuals. Serious efforts are being made to tackle this problem. One such approach is to look for chemical entities from traditionally used medicinal plants. We have examined the effect of the compounds of *R. serpentina* against caspase-8, BACE, and AChE, the well-known targets of NDs. The virtual screening of several compounds was performed along with the toxicological profile, ADME properties, and pharmacokinetics. The screening data led to the identification of alstonine and rauwolscine as hit compounds. Only a few compounds of this plant exhibited Ames toxicity, and none were predicted to show oral rat acute toxicity and inhibition of hERG I. Both the compounds were predicted to be active against neurodegenerative diseases and AD. Alstonine and rauwolscine showed strong affinity toward the target proteins and interacted at their respective active sites. Molecular simulation analysis confirmed the stable nature of both the ligands with all three target proteins under physiological conditions. This study highlights the potential of alstonine and rauwolscine in the management of NDs, and these compounds could be developed as effective drugs after careful *in vivo* examination.

FUNDING

This project was funded by King Salman Center for Disability Research, Research Group no: KSRG-2023-194.

AUTHOR CONTRIBUTIONS

All authors contributed equally to this paper.

CONFLICTS OF INTEREST

The authors declare no conflicts of interest in association with the present study.

ACKNOWLEDGMENTS

The authors extend their appreciation to the King Salman Center for Disability Research for funding this work through Research Group no KSRG-2023-194.

REFERENCES

Ahmad S.S., Sinha M., Ahmad K., Khalid M. and Choi I. (2020). Study of caspase 8 inhibition for the management of Alzheimer's disease: a molecular docking and dynamics simulation. *Molecules*, 25, 2071. 10.3390/molecules25092071.

Ali W.B., Shireen E., Masroor M., Kiran S., Memon N., Junaid N., et al. (2022). Oral administration of *Rauwolfia serpentina* plant extract mitigated immobilization stress-induced behavioral and biochemic and deficits in rats. *Biol. Life Sci. Forum*, 12(1), 32. 10.3390/IECN2022-12393.

Arulraj R., Sivakumar S., Suresh S. and Anitha K. (2020). Synthesis, vibrational spectra, DFT calculations, Hirshfeld surface analysis and molecular docking study of 3-chloro-3-methyl-2,6-diphenylpiperidin-4-one. *Spectrochim. Acta Part A Mol. Biomol. Spectrosc.*, 232, 118166. 10.1016/j.saa.2020.118166.

Berendsen H.J.C., van der Spoel D. and van Drunen R. (1995). GROMACS: a message-passing parallel molecular dynamics implementation. *Comput. Phys. Commun.*, 91, 43-56. 10.1016/0010-4655(95)00042-E.

Choonara Y., Pillay V., Du Toit L., Modi G., Naidoo D., Ndesendo V., et al. (2009). Trends in the molecular pathogenesis and clinical therapeutics of common neurodegenerative disorders. *Int. J. Mol. Sci.*, 10, 2510-2557. 10.3390/ijms10062510.

Costa-Campos L., Lara D., Nunes D. and Elisabetsky E. (1998). Antipsychotic-like profile of alstonine. *Pharmacol. Biochem. Behav.*, 60, 133-141. 10.1016/S0091-3057(97)00594-7.

Costa-Campos L., Dassoler S.C., Rigo A.P., Iwu M. and Elisabetsky E. (2004). Anxiolytic properties of the antipsychotic alkaloid alstonine. *Pharmacol. Biochem. Behav.*, 77, 481-489. 10.1016/j.pbb.2003.12.002.

Cotman C.W., Poon W.W., Rissman R.A. and Blurton-Jones M. (2005). The role of caspase cleavage of tau in Alzheimer disease neuropathology. *J. Neuropathol. Exp. Neurol.*, 64, 104-112. 10.1093/jnen/64.2.104.

Daina A., Michielin O. and Zoete V. (2017). SwissADME: a free web tool to evaluate pharmacokinetics, drug-likeness and medicinal chemistry friendliness of small molecules. *Sci. Rep.*, 7, 42717. 10.1038/srep42717.

Dey A. and De J. (2011). Ethnobotanical aspects of *Rauvolfia serpentina* (L). Benth. ex kurz. in India, Nepal and Bangladesh. *J. Med. Plant Res.*, 5, 144-150.

Faghihi M.A., Modarresi F., Khalil A.M., Wood D.E., Sahagan B.G., Morgan T.E., et al. (2008). Expression of a noncoding RNA is elevated in Alzheimer's disease and drives rapid feed-forward regulation of β-secretase. *Nat. Med.* 14, 723-730. 10.1038/nm1784.

Filimonov D.A., Lagunin A.A., Gloriozova T.A., Rudik A. V., Druzhilovskii D.S., Pogodin P.V., et al. (2014). Prediction of the biological activity spectra of organic compounds using the pass online web resource. *Chem. Heterocycl. Compd.*, 50, 444-457. 10.1007/s10593-014-1496-1.

Fouedjou R.T., Chtita S., Bakhouch M., Belaidi S., Ouassaf M., Djoumbissie L.A., et al. (2021). Cameroonian medicinal plants as potential candidates of SARS-CoV-2 inhibitors. *J. Biomol. Struct. Dyn.*, 1-15. 10.1080/07391102.2021.1914170.

Ganat Y.M., Silbereis J., Cave C., Ngu H., Anderson G.M., Ohkubo Y., et al. (2006). Early postnatal astroglial cells produce multilineage precursors and neural stem cells in vivo. *J. Neurosci.*, 26, 8609-8621. 10.1523/JNEUROSCI.2532-06.2006.

Ghose A.K., Viswanadhan V.N. and Wendoloski J.J. (1999). A knowledge-based approach in designing combinatorial or medicinal chemistry libraries for drug discovery. 1. A qualitative and quantitative characterization of known drug databases. *J. Comb. Chem.*, 1, 55-68. 10.1021/cc9800071.

Goedert M. and Spillantini M.G. (2006). A century of Alzheimer's disease. *Science*, 314, 777-781. 10.1126/science.1132814.

Hoover B.R., Reed M.N., Su J., Penrod R.D., Kotilinek L.A., Grant M.K., et al. (2010). Tau mislocalization to dendritic spines mediates synaptic dysfunction independently of neurodegeneration. *Neuron*, 68, 1067-1081. 10.1016/j.neuron.2010.11.030.

Iqbal D., Rehman M.T., Alajmi M.F., Alsaweed M., Jamal Q.M.S., Alasiry S.M., et al. (2023). Multitargeted virtual screening and molecular simulation of natural product-like compounds against GSK3β, NMDA-receptor, and BACE-1 for the management of Alzheimer's disease. *Pharmaceuticals*, 16, 622. 10.3390/ph16040622.

Itoh A., Kumashiro T., Yamaguchi M., Nagakura N., Mizushina Y., Nishi T., et al. (2005). Indole alkaloids and other constituents of *Rauwolfia serpentina*. *J. Nat. Prod.*, 68, 848-852. 10.1021/np058007n.

Jamal S., Grover A. and Grover S. (2019). Machine learning from molecular dynamics trajectories to predict caspase-8 inhibitors against *Alzheimer's disease*. *Front. Pharmacol.*, 10, 780. 10.3389/fphar.2019.00780.

Jefferys J. and Cooper A. (2007). Brain basics. The human brain and its disorders. 1-20.

Kametani F. and Hasegawa M. (2018). Reconsideration of amyloid hypothesis and tau hypothesis in Alzheimer's disease. *Front. Neurosci.*, 12, 25. 10.3389/fnins.2018.00025.

Kovacs G.G. (2019). Molecular pathology of neurodegenerative diseases: principles and practice. *J. Clin. Pathol.*, 72, 725-735. 10.1136/jclinpath-2019-205952.

Kumari R., Rathi B., Rani A. and Bhatnagar S. (2013). *Rauvolfia serpentina* L. Benth. ex Kurz.: phytochemical, pharmacological and therapeutic aspects. *Int. J. Pharm. Sci. Rev. Res.*, 23, 348-55.

Kumari R., Kumar R. and Lynn A. (2014). g_mmpbsa —A GROMACS tool for high-throughput MM-PBSA calculations. *J. Chem. Inf. Model.*, 54, 1951-1962. 10.1021/ci500020m.

Kumari I., Walia B. and Chaudhary G. (2021). *Rauwolfia serpentina* (sarpgandha): a review based upon its phytochemistry and ayurvedic uses. *Int. J. Curr. Res.*, 13, 16727-16734.

Lamptey R.N.L., Chaulagain B., Trivedi R., Gothwal A., Layek B. and Singh J. (2022). A review of the common neurodegenerative disorders: current therapeutic approaches and the potential role of nanotherapeutics. *Int. J. Mol. Sci.*, 23, 1851. 10.3390/ijms23031851.

Lipinski C.A. (2004). Lead- and drug-like compounds: the rule-of-five revolution. *Drug Discov. Today Technol.*, 1, 337-341. 10.1016/j.ddtec.2004.11.007.

Martin J.B. (1999). Molecular basis of the neurodegenerative disorders. *N. Engl. J. Med.* 340, 1970-1980. 10.1056/NEJM199906243402507.

Merelli A., Czornyj L. and Lazarowski A. (2013). Erythropoietin: a neuroprotective agent in cerebral hypoxia, neurodegeneration, and epilepsy. *Curr. Pharm. Des.*, 19, 6791-6801. 10.2174/1381612811319380011.

Milnerwood A.J. and Raymond L.A. (2010). Early synaptic pathophysiology in neurodegeneration: insights from Huntington's disease. *Trends Neurosci.*, 33, 513-523. 10.1016/j.tins.2010.08.002.

Morris G.M., Huey R., Lindstrom W., Sanner M.F., Belew R.K., Goodsell D.S., et al. (2009). AutoDock4 and AutoDockTools4: automated docking with selective receptor flexibility. *J. Comput. Chem.*, 30, 2785-2791. 10.1002/jcc.21256.

Mouchlis V.D., Melagraki G., Zacharia L.C. and Afantitis A. (2020). Computer-aided drug design of β-secretase, γ-secretase and anti-tau inhibitors for the discovery of novel Alzheimer's therapeutics. *Int. J. Mol. Sci.*, 21, 703. 10.3390/ijms21030703.

Parrinello M. and Rahman A. (1981). Polymorphic transitions in single crystals: a new molecular dynamics method. *J. Appl. Phys.*, 52, 7182-7190. 10.1063/1.328693.

Pathania S., Ramakrishnan S.M., Randhawa V. and Bagler G. (2015). SerpentinaDB: a database of plant-derived molecules of *Rauvolfia serpentina*. *BMC Complement. Altern. Med.*, 15, 262. 10.1186/s12906-015-0683-7.

Pires D.E.V., Blundell T.L. and Ascher D.B. (2015). pkCSM: predicting small-molecule pharmacokinetic and toxicity properties using graph-based signatures. *J. Med. Chem.*, 58, 4066-4072. 10.1021/acs.jmedchem.5b00104.

Przedborski S., Vila M. and Jackson-Lewis V. (2003). Series introduction: neurodegeneration: what is it and where are we? *J. Clin. Invest.*, 111, 3-10. 10.1172/JCI200317522.

Qais F.A., Sarwar T., Ahmad I., Khan R.A., Shahzad S.A. and Husain F.M. (2021). Glyburide inhibits non-enzymatic glycation of HSA: an approach for the management of AGEs associated diabetic complications. *Int. J. Biol. Macromol.*, 169, 143-152. 10.1016/j.ijbiomac.2020.12.096.

Qais F.A., Ahmad I., Husain F.M., Arshad M., Khan A. and Adil M. (2023). Umbelliferone modulates the quorum sensing and biofilm of Gram −ve bacteria: in vitro and in silico investigations. *J. Biomol. Struct. Dyn.*, 1-14. 10.1080/07391102.2023.2229454.

Qian M., Liu J., Yao J., Wang W., Yang J., Wei L., et al. (2015). Caspase-8 mediates amyloid-β-induced apoptosis in differentiated PC12 cells. *J. Mol. Neurosci.*, 56, 491-499. 10.1007/s12031-015-0498-5.

Qureshi S. and Udani S. (2009). Hypolipidaemic activity of *Rauwolfia serpentina* Benth. *Pakistan J. Nutr.*, 8, 1103-1106.

Rapp T., Chauvin P., Costa N. and Molinier L. (2015). Health economic considerations in neurodegenerative disorders. In: *Imaging Neurodegener*. pp. 42-53, Disord., Oxford University Press. 10.1093/med/9780199671618.003.0004.

Rath B., Qais F.A., Patro R., Mohapatra S. and Sharma T. (2021). Design, synthesis and molecular modeling studies of novel mesalamine linked coumarin for treatment of inflammatory bowel disease. *Bioorg. Med. Chem. Lett.*, 41, 128029. 10.1016/j.bmcl.2021.128029.

Ruz C., Alcantud J.L., Vives Montero F., Duran R. and Bandres-Ciga S. (2020). Proteotoxicity and neurodegenerative diseases. *Int. J. Mol. Sci.*, 21, 5646. 10.3390/ijms21165646.

Šali A. and Blundell T.L. (1993). Comparative protein modelling by satisfaction of spatial restraints. *J. Mol. Biol.*, 234, 779-815. 10.1006/jmbi.1993.1626.

Sayad A., Najafi S., Hussen B.M., Abdullah S.T., Movahedpour A., Taheri M., et al. (2022). The emerging roles of the β-secretase BACE1 and the long non-coding RNA BACE1-AS in human diseases: a focus on neurodegenerative diseases and cancer. *Front. Aging Neurosci.*, 14, 853180. 10.3389/fnagi.2022.853180.

Scott D.A., Tabarean I., Tang Y., Cartier A., Masliah E. and Roy S. (2010). A pathologic cascade leading to synaptic dysfunction in -synuclein-induced neurodegeneration. *J. Neurosci.*, 30, 8083-8095. 10.1523/JNEUROSCI.1091-10.2010.

Siddiqui S., Ameen F., Kausar T., Nayeem S.M., Ur Rehman S. and Tabish M. (2021). Biophysical insight into the binding mechanism of doxofylline to bovine serum albumin: an in vitro and in silico approach. *Spectrochim. Acta Part A Mol. Biomol. Spectrosc.*, 249, 119296. 10.1016/j.saa.2020.119296.

Sousa da Silva A.W. and Vranken W.F. (2012). ACPYPE – AnteChamber PYthon Parser interfacE. *BMC Res. Notes*, 5, 367. 10.1186/1756-0500-5-367.

Tiwari S. (2008). Plants: a rich source of herbal medicine. *J. Nat. Prod.*, 1, 27-35.

Trivedi S., Kumar V., Singh S. and Kumar M. (2021). Efficacy evaluation of *Rauwolfia serpentina* against Chromium (VI) toxicity in fish, Channa punctatus. *J. Environ. Biol.*, 42, 659-667.

Trott O. and Olson A.J. (2009). AutoDock Vina: improving the speed and accuracy of docking with a new scoring function, efficient optimization, and multithreading. *J. Comput. Chem.*, 31, 455-461. 10.1002/jcc.21334.

van den Heuvel M.P. and Sporns O. (2013). Network hubs in the human brain. *Trends Cogn. Sci.*, 17, 683-696. 10.1016/j.tics.2013.09.012.

Walczak-Nowicka Ł.J. and Herbet M. (2021). Acetylcholinesterase inhibitors in the treatment of neurodegenerative diseases and the role of acetylcholinesterase in their pathogenesis. *Int. J. Mol. Sci.*, 22, 9290. 10.3390/ijms22179290.

Wang J., Wolf R.M., Caldwell J.W., Kollman P.A. and Case D.A. (2004). Development and testing of a general amber force field. *J. Comput. Chem.*, 25, 1157-1174. 10.1002/jcc.20035.

Wang Y., Xing J., Xu Y., Zhou N., Peng J., Xiong Z., et al. (2015). In silico ADME/T modelling for rational drug design. *Q. Rev. Biophys.*, 48, 488-515. 10.1017/S0033583515000190.